JOURNAL OF PROPULSION AND POWER
Vol. 19, No. 4, July–August 2003

Evaluating Experimental Data Requirements for Spatially Varying Turbine Flowfields Through Uncertainty Analysis

Susan T. Hudson*
Mississippi State University, Mississippi State, Mississippi 39762
and
Boon Liang Heng†
Imation Corporation, Camarillo, California 93011

Experimental data from two cold-airflow turbine tests were evaluated. The two tests had different, relatively high spatial variations in the turbine exit flowfields. The objective of the research was to evaluate data requirements, including the averaging techniques, the number of measurements (spatial resolution), and the types of measurements needed, to obtain high-quality performance and code validation data for these types of flowfields. Uncertainty analysis methodology was used, and new uncertainty techniques were developed for the data studies. The results were then used to establish guidelines for planning future tests of other turbines. The guidelines set forth a quantified method for determining data requirements to meet specified test goals. Implementation of these guidelines will improve the quality of experimental results while decreasing time and cost for experimental studies of highly nonuniform turbine flowfields.

Nomenclature

B	=	systematic uncertainty estimate
C_p	=	specific heat at constant pressure
h	=	enthalpy
M	=	Mach number
N	=	speed
P	=	random uncertainty estimate
$\bar{P}$	=	pressure
P_r	=	pressure ratio
r	=	result
T	=	temperature
U	=	uncertainty estimate
X	=	measured variable
α	=	flow or yaw angle
γ	=	ratio of specific heats
η	=	efficiency
θ	=	partial derivative

Subscripts

av	=	average
c	=	dummy variable
th	=	thermodynamic method
t-t	=	total-to-total
0	=	total
1	=	turbine inlet
2	=	turbine exit

Introduction

UNDERSTANDING the turbine flowfield is an important aspect in characterizing the turbine aerodynamic performance. Component testing of new turbine designs to determine these flowfields is often done under scaled conditions, which allows a broader test envelope.[1] This type of experimental work is particularly important for designs incorporating revolutionary concepts in an attempt to improve performance while reducing weight and cost.

This paper is a study of the experimental data obtained from the oxidizer technology turbine rig (OTTR), which was designed to support the development of advanced turbines for future liquid rocket engines.[2] The experimental results were used to validate various computational fluid dynamics codes used for design and performance prediction. Therefore, the experimental uncertainty requirements were strict, and the uncertainty goal for the turbine efficiency was 1% ($U_\eta/\eta \times 100 = \pm 1\%$).

Experimental data from two cold-airflow turbine tests were evaluated. The first OTTR test was with a square exit volute. The oversized exit volute was a square cross-sectional area to increase the volute flow area so that the turbine could be evaluated over a large offdesign envelope. This prevented the flow from choking in the exit volute before flow choked in the turbine at the offdesign conditions. The second OTTR test used an exit volute with a circular cross-sectional area to best match the turbine exit flowfield for optimum performance. These two exit volutes created different and relatively high spatial variations in the turbine exit flowfields.

The objective of the research was to evaluate data requirements, including the averaging techniques, the number of measurements (spatial resolution), and the types of measurements needed for flowfields with large spatial variations. Several different data studies were conducted to meet the objective. A large quantity of data was collected for the two tests in this study. These test data were then reduced in various ways for the data studies. An uncertainty analysis approach was used, and all evaluations were made relative to the uncertainty goal for determining turbine efficiency. The first data study was a comparison between mass and area averaging of the measured variables needed to calculate turbine efficiency. The second data study involved reducing the number of point measurements made to obtain the average values of the measured variables needed to calculate turbine efficiency. Finally, the types of static pressure measurements required to calculate efficiency were evaluated. A new uncertainty analysis technique was developed to include conceptual bias estimates properly for the spatially averaged values required in the efficiency equations. This technique was crucial in obtaining valid uncertainty estimates for the various cases.

Conclusions were drawn for the OTTR test results. These results were then generalized to provide guidelines for future tests of other

Presented as Paper 2002-0883 at the 40th Aero. Science Meeting, **XXXX**; received 11 March 2002; revision received 14 April 2003; accepted for publication 17 April 2003.

*Adjunct Assistant Professor, Mechanical Engineering Department, 210 Carpenter, Mississippi State, MS 39762, and Director of Engineering, Drives and Controls Specialties, Inc., 545 W. Bobo Newsom Highway, Hartsville, SC 29550. Associate Fellow AIAA.

†Process Engineer, Data Storage and Information Management, P.O. Box 2378. Member AIAA.

turbines. The uncertainty analysis techniques developed permit a better understanding of the measurements and analysis methods required to meet the test goals. Application of the guidelines presented here will improve the quality of experimental results, while decreasing time and cost for turbines with large spatial variations.

This paper begins with defining turbine efficiency for this work. Next, the test facility, turbine model and instrumentation, and test conditions are presented to provide the necessary background information. Then the data studies and uncertainty analysis methodology are described. Results of the data studies are subsequently shown and discussed. Finally, conclusions for the OTTR test, as well as generalized results to provide guidelines for future turbine testing, are given.

Turbine Efficiency

To develop test guidelines to meet specific uncertainty goals, the turbine flowfields and data analysis methods were studied. Two equations used to calculate turbine efficiency from measured test variables were evaluated during this study.[3,4] The two methods used were the thermodynamic method and the mechanical method.[5,6] Both equations are derived from the basic definition of turbine efficiency: actual enthalpy change over ideal or isentropic enthalpy change. Both methods are used for "cold"-airflow turbine testing where the temperature is relatively low so that an ideal gas may be assumed and γ and C_p are considered constant. However, because the general trends and conclusions drawn from the data were the same for both methods, results from only the thermodynamic method will be presented.

For this efficiency method, the temperature drop across the turbine is measured to determine the actual enthalpy change ($\Delta h = C_p \Delta T$). Isentropic relations are used to relate the ideal enthalpy change in terms of the turbine inlet and exit total pressures rather than the temperatures. With these assumptions, the equation for thermodynamic efficiency becomes

$$\eta_{\text{th}} = \frac{T_{01} - T_{02}}{T_{01}\left[1 - (\bar{P}_{02}/\bar{P}_{01})^{(\gamma-1)/\gamma}\right]} \tag{1}$$

Note that the temperatures and pressures in Eq. (1) are average values at a cross section (turbine inlet and exit), yet individual point measurements of pressure and temperature must be made. These individual measurements must then be averaged to obtain the values required in the equation. This idea will be important for the data studies results and conceptual bias estimates to be discussed later.

Description of Experiment

The turbine was a highly loaded single-stage oxidizer turbine that used inlet and exit volutes to provide optimum performance in a compact configuration.[2] The aerodynamic design was incorporated into a turbine test rig, the OTTR, and tested in the Marshall Space Flight Center's cold-airflow turbine test equipment (TTE). The rig was heavily instrumented to obtain a benchmark quality data set.[7–9]

Facility Description

The TTE is a blowdown facility that operates by expanding high-pressure air [420 psig (2896 kPa)] from one or two 6000-ft^3 (170-m^3) air tanks to atmospheric conditions.[10] Air flows from the storage tanks through a heater section, a quiet trim control valve, and a calibrated subsonic mass flow venturi. Flow then continues through the test model and backpressure valve and exhausts to atmosphere. Flow straighteners are used in the piping upstream of the test model. Two inlet pipe sections containing four bosses [2 in. (5 cm) diam] each are also included for facility measurements and seeding for laser Doppler velocimetry measurements. The facility can accommodate axial flow, radial inflow, and radial outflow turbines.

This equipment can deliver up to 220-psia (1517-kPa) air for run times from 30 s to over 1 h, depending on inlet pressure and mass flow rate. The heater allows a blowdown controlled temperature between 530 (294) and 830°R (461 K). The TTE has manual set point closed-loop control of the model inlet total pressure, inlet total temperature, shaft rotational speed, and pressure ratio. The facility accurately measures mass flow rate, torque, and horsepower. The data acquisition system is capable of measuring 512 pressures, 120 temperatures, and several model health monitoring variables.

Model Description and Instrumentation

The OTTR model, shown in Fig. 1 and 2, was divided into the inlet volute, turbine stage, exit volute, and diffuser sections.[2,11] The inlet volute routed the conditioned air from the TTE through the turbine section. The single-stage turbine had 20 vanes and 42 blades rotating clockwise when viewed from aft looking upstream. The turbine blades (Fig. 1) had a turning angle of 157 deg. After the turbine section, flow was guided through the exit volute and the diffuser. Both exit volutes tested were configured to be 139 deg away from the inlet volute (Fig. 2).

The rig instrumentation was similar for both the square and circular exit volute tests. This instrumentation was planned so that the performance of each section (inlet volute, turbine, exit volute, and diffuser) could be evaluated. The instrumentation at the inlet and exit planes of the turbine section is the focus of this paper. Data at these planes were taken using total pressure and total temperature rakes, three-hole cobra probes on radial traverse actuators, and a three-hole modified prism (YC) probe. This instrumentation was installed on rotating rings. Each ring held eight rakes and two probes with radial actuators. The total pressure and total temperature rakes contained five probes positioned on centers of equal area within the turbine inlet and exit (Fig. 3). The yaw angles of the rakes were adjusted

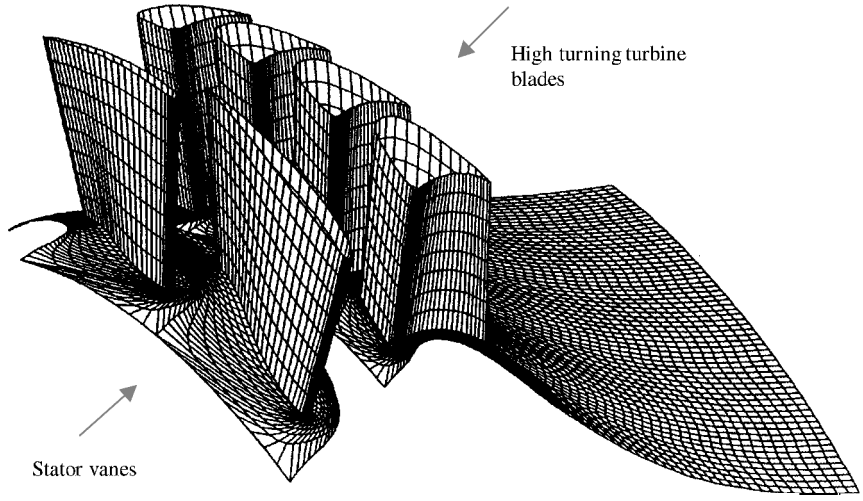

Fig. 1 OTTR vanes and blades.

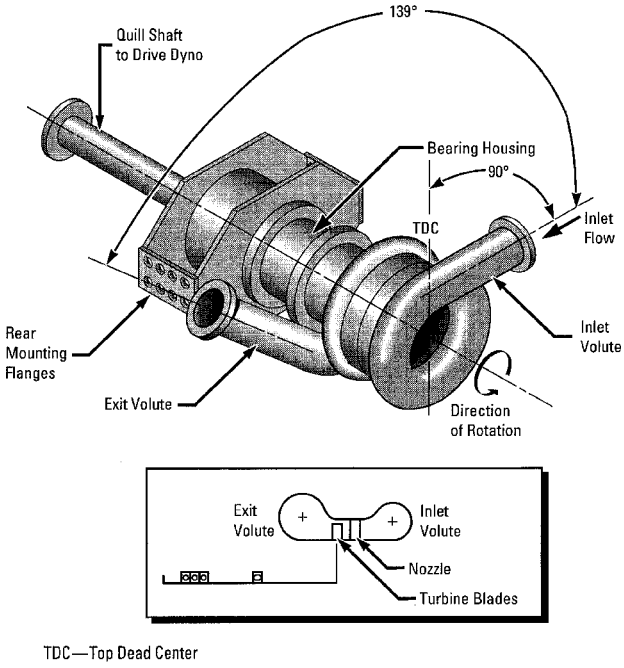

Fig. 2 OTTR schematic.

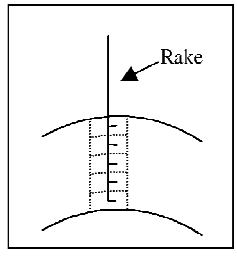

Rake with 5 probes positioned on centers of equal area.

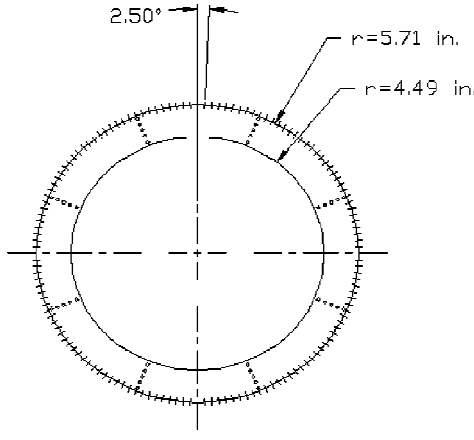

Fig. 3 OTTR inlet and exit instrumentation.

manually. An automatic traverse gear moved the ring through 90 deg circumferentially at the turbine inlet and exit.

Eight equally spaced wall static pressures were placed on the turbine inner and outer diameters at the turbine inlet and exit. The i.d. wall static pressures were fixed; however, the o.d. static pressures were located on the rotating ring and moved with the ring.

The three-hole probes were carefully calibrated to obtain yaw angle, total pressure, and static pressure.[5] The cobra probes were mounted on radial traverse actuators so that the radial position could be automatically set and adjusted during test runs. The cobra probes also operated in an "autonulling" mode meaning that they automatically adjusted to the angle of the incoming flow. (The pressures of the two side ports were equal.) Therefore, the only correction necessary to obtain flow angle with a cobra probe was to apply the "offset" (the difference between the aerodynamic null point and the geometric null point), which was determined from calibration for the particular probe at 0 deg, to the flow angle recorded when the probe autonulled. Because the cobra probes were always aligned with the incoming flow, they could be used to obtain static pressure if properly calibrated. For static and total pressures, the cobra probes were calibrated at 0 deg over a Mach number range ($0.16 \leq M \leq 0.90$). The cobra probes were used to map only two 90-deg quadrants of the turbine inlet and exit planes because the casings had to be open to accommodate the radial actuators. Obviously, the entire 360 deg could not be open: The two 90-deg quadrant openings were dictated by structural guidelines. The two quadrants mapped by the cobra probes are shown in Fig. 4.

The remaining two quadrants of the turbine exit plane were mapped using the YC probe. The YC probe stem was short so that it could be mounted in any pressure or temperature rake position. With this design, it could move under the closed sections of the casing covering the entire 360 deg. However, because the YC probe had to be manually set for both radial position and yaw angle, it was much more difficult to use and consumed much more test time. The YC probe required the calibrations mentioned earlier for the cobra probes, as well as calibration data over a yaw angle range ($-15 \leq \alpha \leq +15$), because it could not autonull. The YC probe was chosen for these measurements over other three-hole probes such as cobra probes because its design was better for obtaining static pressure when the probe was not aligned with the flow. The YC probe coverage is shown in Fig. 4. The YC and cobra probe measurements overlapped through two 22.5-deg sections (Fig. 4). Hence, two 22.5-deg sections of the turbine exit were not measured (Fig. 4). Data in these two sections were filled using linear regressions.

The ring rotation along with the number of rakes and probes permitted measurements of total pressure, total temperature, static pressure, and yaw angle over the entire 360 deg of the turbine inlet and exit planes (Fig. 3). Because no information was available before these tests on the number of measurements needed, the maximum number of independent measurements possible based on probe size were taken. Measurements were taken every 2.5 deg creating

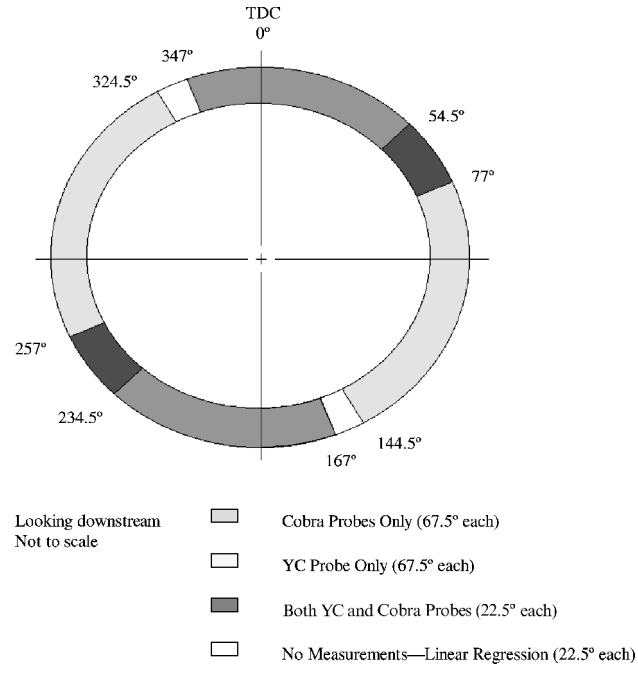

Fig. 4 Three-hole probe coverage of the turbine exit plane.

720-point measurements of total pressure, total temperature, static pressure, and yaw angle at the turbine inlet and exit. The instrumentation plans used during testing to obtain these measurements were based on previous probe interference and rake blockage studies with the test model.[12]

Test Conditions

The OTTR was tested at the turbine aerodynamic design point (ADP) and over a broad offdesign operating range. The ADP test conditions are the emphasis of this paper. The TTE setpoint parameters at ADP were $\bar{P}_{0_1} = 100$ psia (689 kPa), $T_{0_1} = 560°$R (311 K), $N = 3710$ rpm, and $P_{r\,t\text{-}t} = 1.60$ for both tests.[5,9,13,14]

Data Studies

Several different data studies were conducted. The experimental results using the 720-point measurements and mass averaging at the turbine exit were considered the "best" results or "true" values and were the basis of comparison for all studies. (Note that the turbine inlet quantities were always area averaged based on previous findings that mass averaging was not required for the relatively uniform flow at the inlet.[5,9,13,14]) In all cases, the turbine efficiency and the uncertainty of the turbine efficiency were calculated to make the comparisons.

The first data study was a comparison between mass and area averaging at the turbine exit. Area averaging is much simpler than mass averaging because the probes can be placed on centers of equal area. When this is done, the area average is simply a numerical average. However, a weighting factor based on mass flow rate must be obtained to mass average. Determination of the weighting factor requires measurements of total pressure, total temperature, yaw angle, and static pressure. Obtaining the measurements needed for mass averaging greatly increases probe calibration requirements and test time.

The second data study involved reducing the number of point measurements from 720. This study had several different aspects. First, the number of data points was reduced from 720 to 360 to 180 to 90 while maintaining full 360-deg circumferential coverage. This was accomplished by simply deleting measured data points in equal increments from the analysis as if they had not been made. Next, coverage of specific quadrants was considered. As already noted, the cobra probes on radial actuators could only be used in two 90-deg quadrants due to structural constraints, and testing with the modified YC probe was much more time consuming and costly. Therefore, this study was conducted to determine if the additional time and effort required using the YC probe for full 360-deg coverage was necessary. The two quadrants covered by the cobra probes were used in one case, and the two quadrants covered by the YC probe were used in another case. Calculations were made for 720, 360, 180, and 90 data points for the quadrants coverage just as with the full 360-deg coverage.

Finally, an evaluation of the types of measurements required was done. Obtaining the static pressure measurements across the annulus is much more difficult and time consuming than obtaining wall static pressure measurements due to increased probe calibration requirements and test time. Therefore, a comparison between these two means of obtaining static pressure was made. When the wall static pressure measurements were used, the average value was obtained in two different ways. First, simply a numerical average of all of the i.d. and o.d. values was used [numerical wall average (NWA)]. Second, the i.d. and o.d. values at each circumferential position were averaged, and the value at that particular position was used to obtain the weighting factor for mass averaging [circumferential wall average (CWA)]. This method accounted for the circumferential variation in static pressure in the mass averaging.

Uncertainty Analysis Methodology

Uncertainty analysis techniques were used for the data studies discussed. The general methodology followed is described in Refs. 15 and 16. A brief overview of basic uncertainty analysis will be presented in this section. The uncertainty analysis techniques developed for this study will then be reviewed. Further details of the uncertainty analyses for this study may be obtained from Refs. 5, 6, and 9.

The word accuracy is generally used to indicate the relative closeness of agreement between an experimentally determined value of a quantity and its true value. Error is the difference between the experimentally determined value and the truth; therefore, as error decreases, accuracy is said to increase. Only in rare instances is the true value of a quantity known. Thus, it is necessary to estimate error, and that estimate is called an uncertainty U. Uncertainty estimates are made at some confidence level: A 95% confidence estimate, for example, means that the true value of the quantity is expected to be within the $\pm U$ interval about the experimentally determined value 95 times out of 100.

Total error can be considered to be composed of two components: a random (precision) component and a systematic (bias) component. An error is classified as random if it contributes to the scatter of the data; otherwise, it is a systematic error. In nearly all experiments, the measured values of different variables are combined using a data reduction equation (DRE) to form some desired result. A general representation of a DRE is

$$r = r(X_1, X_2, \ldots, X_J) \tag{2}$$

where r is the experimental result determined from J measured variables X_J. Each of the measured variables contains systematic errors and random errors. These errors in the measured values then propagate through the data reduction equation, thereby generating the systematic and random errors in the experimental result, r.

If the large sample assumption is made,[15] then the 95% confidence expression for U_r becomes

$$U_r^2 = B_r^2 + P_r^2 \tag{3}$$

The systematic uncertainty (bias limit) of the result is

$$B_r^2 = \sum_{i=1}^{J} \theta_i^2 B_i^2 + 2 \sum_{i=1}^{J-1} \sum_{k=i+1}^{J} \theta_i \theta_k B_{ik} \tag{4}$$

The θ_i are the partial derivatives of each measured variable defined as

$$\theta_i = \frac{\partial r}{\partial X_i} \tag{5}$$

The random uncertainty (precision limit) of the result is

$$P_r^2 = \sum_{i=1}^{J} \theta_i^2 P_i^2 + 2 \sum_{i=1}^{J-1} \sum_{k=i+1}^{J} \theta_i \theta_k P_{ik} \tag{6}$$

The B_i and P_i terms are the bias limit and precision limit estimates, respectively, for each X_i measured variable. The B_{ik} and P_{ik} terms are the 95% confidence estimates of the covariance terms and account for errors that are common between different measured variables.

The detailed uncertainty analysis method for the OTTR was developed to account for explicitly the averaging procedures used to calculate efficiency (mass and area averaging). The DRE, η_{th}, was written explicitly in terms of the measured variables and averaging procedures. According to Eq. (1), the thermodynamic efficiency is a function of $\bar{P}_{01}$, $\bar{P}_{02}$, T_{01}, and T_{02} (Refs. 3–5). However, static pressure and flow angle measurements were needed for the mass averaging technique. Hence, the efficiency equation is a function of the following:

$$\eta_{\text{th}} = \eta_{\text{th}} \left[\sum_{i=1}^{720} (\bar{P}_{01}, \bar{P}_{02}, T_{01}, T_{02}, P_2, \alpha_2)_i \right] \tag{7}$$

Combining Eq. (7) with Eqs. (3), (4), and (6), the equation for uncertainty in thermodynamic efficiency becomes

$$
\begin{aligned}
U_{\eta_{\text{th}}}^2 = {} & \sum_{i=1}^{720}\left(\frac{\partial\eta}{\partial\bar{P}_{01i}}P_{\bar{P}_{01i}}\right)^2 + \sum_{i=1}^{720}\left(\frac{\partial\eta}{\partial\bar{P}_{02i}}P_{\bar{P}_{02i}}\right)^2 \\
& + \sum_{i=1}^{720}\left(\frac{\partial\eta}{\partial T_{01i}}P_{T_{01i}}\right)^2 + \sum_{i=1}^{720}\left(\frac{\partial\eta}{\partial T_{02i}}P_{T_{02i}}\right)^2 \\
& + \sum_{i=1}^{720}\left(\frac{\partial\eta}{\partial\bar{P}_{2i}}P_{\bar{P}_{2i}}\right)^2 + \sum_{i=1}^{720}\left(\frac{\partial\eta}{\partial\alpha_{2i}}P_{\alpha_{2i}}\right)^2 \\
& + \sum_{i=1}^{720}\left(\frac{\partial\eta}{\partial\bar{P}_{01i}}B_{\bar{P}_{01i}}\right)^2 + \sum_{i=1}^{720}\left(\frac{\partial\eta}{\partial\bar{P}_{02i}}B_{\bar{P}_{02i}}\right)^2 \\
& + \sum_{i=1}^{720}\left(\frac{\partial\eta}{\partial T_{01i}}B_{T_{01i}}\right)^2 + \sum_{i=1}^{720}\left(\frac{\partial\eta}{\partial T_{02i}}B_{T_{02i}}\right)^2 \\
& + \sum_{i=1}^{720}\left(\frac{\partial\eta}{\partial\bar{P}_{2i}}B_{\bar{P}_{2i}}\right)^2 + \sum_{i=1}^{720}\left(\frac{\partial\eta}{\partial\alpha_{2i}}B_{\alpha_{2i}}\right)^2 \\
& + 2\sum_{i=1}^{719}\sum_{j=i+1}^{720}\left(\frac{\partial\eta}{\partial\bar{P}_{01}}\right)_i\left(\frac{\partial\eta}{\partial\bar{P}_{01}}\right)_j B_{\bar{P}_{01i}\bar{P}_{01j}} \\
& + 2\sum_{i=1}^{719}\sum_{j=i+1}^{720}\left(\frac{\partial\eta}{\partial\bar{P}_{02}}\right)_i\left(\frac{\partial\eta}{\partial\bar{P}_{02}}\right)_j B_{\bar{P}_{02i}\bar{P}_{02j}} \\
& + 2\sum_{i=1}^{719}\sum_{j=i+1}^{720}\left(\frac{\partial\eta}{\partial T_{01}}\right)_i\left(\frac{\partial\eta}{\partial T_{01}}\right)_j B_{T_{01i}T_{01j}} \\
& + 2\sum_{i=1}^{719}\sum_{j=i+1}^{720}\left(\frac{\partial\eta}{\partial T_{02}}\right)_i\left(\frac{\partial\eta}{\partial T_{02}}\right)_j B_{T_{02i}T_{02j}} \\
& + 2\sum_{i=1}^{719}\sum_{j=i+1}^{720}\left(\frac{\partial\eta}{\partial\bar{P}_{2}}\right)_i\left(\frac{\partial\eta}{\partial\bar{P}_{2}}\right)_j B_{\bar{P}_{2i}\bar{P}_{2j}} \\
& + 2\sum_{i=1}^{719}\sum_{j=i+1}^{720}\left(\frac{\partial\eta}{\partial\alpha_{2}}\right)_i\left(\frac{\partial\eta}{\partial\alpha_{2}}\right)_j B_{\alpha_{2i}\alpha_{2j}} \\
& + 2\sum_{i=1}^{720}\sum_{j=1}^{720}\left(\frac{\partial\eta}{\partial\bar{P}_{01}}\right)_i\left(\frac{\partial\eta}{\partial\bar{P}_{02}}\right)_j B_{\bar{P}_{01i}\bar{P}_{02j}} \\
& + 2\sum_{i=1}^{720}\sum_{j=1}^{720}\left(\frac{\partial\eta}{\partial\bar{P}_{01}}\right)_i\left(\frac{\partial\eta}{\partial\bar{P}_{2}}\right)_j B_{\bar{P}_{01i}\bar{P}_{2j}} \\
& + 2\sum_{i=1}^{720}\sum_{j=1}^{720}\left(\frac{\partial\eta}{\partial\bar{P}_{01}}\right)_i\left(\frac{\partial\eta}{\partial\alpha_{2}}\right)_j B_{\bar{P}_{01i}\alpha_{2j}} \\
& + 2\sum_{i=1}^{720}\sum_{j=1}^{720}\left(\frac{\partial\eta}{\partial\bar{P}_{02}}\right)_i\left(\frac{\partial\eta}{\partial\bar{P}_{2}}\right)_j B_{\bar{P}_{02i}\bar{P}_{2j}} \\
& + 2\sum_{i=1}^{720}\sum_{j=1}^{720}\left(\frac{\partial\eta}{\partial\bar{P}_{02}}\right)_i\left(\frac{\partial\eta}{\partial\alpha_{2}}\right)_j B_{\bar{P}_{02i}\alpha_{2j}} \\
& + 2\sum_{i=1}^{720}\sum_{j=1}^{720}\left(\frac{\partial\eta}{\partial T_{01}}\right)_i\left(\frac{\partial\eta}{\partial T_{02}}\right)_j B_{T_{01i}T_{02j}} \\
& + 2\sum_{i=1}^{720}\sum_{j=1}^{720}\left(\frac{\partial\eta}{\partial\bar{P}_{2}}\right)_i\left(\frac{\partial\eta}{\partial\alpha_{2}}\right)_j B_{\bar{P}_{2i}\alpha_{2j}} \qquad (8)
\end{aligned}
$$

The efficiency uncertainty equation accounts for the number of point measurements, averaging procedure, conc. bias, and correlation of the measured variables in the OTTR test. The equation was divided into four major portions. The first 6 uncertainty terms on the right-hand side were the random terms for each measured variable, the 7th–12th terms were the systematic terms for each variable, the 13th–18th terms were the correlated systematic terms between point measurements for the same variable, and the 19th–25th terms were the correlated systematic terms for point measurements of different variables. All correlated random terms were set to zero.[5,6,13] Further details on the uncertainty equation may be obtained from Refs. 5 and 6.

An uncertainty analysis idea that is crucial in this work is the conceptual bias. In this work, Eq. (8) was modified to accommodate conceptual bias estimates. A conceptual bias results when the values required for an equation differ from the values that can actually be measured.[5,9,15] As already noted, the total pressure and total temperatures in the turbine efficiency equation are average values at a cross section; nevertheless, point measurements of pressure and temperature must be made. These point measurements must then be averaged to obtain the values for the equations. The number of measurements made and the averaging procedure used will obviously affect these values, as well as the uncertainties of these values. Conceptual bias, therefore, in this case is the bias that arises when a cross-sectional average value required in the DRE is replaced by an average of multiple point measurements. The cross-sectional average is the integral; however, a summation of values must be made to approximate the integral. If enough measurements are made, then the summation is approximately equal to the integral, and the conceptual bias error is negligible. However, how does one determine how many measurements are required to make the conceptual bias error negligible? The work described here attempts to help answer that question. Because 720 measurements were the maximum number of truly independent spatial measurements possible given the annulus area and probe dimensions for the OTTR, it was assumed that conceptual bias error was negligible when 720 measurements were properly averaged to obtain the values ($\sum \approx \int$). Hence, these values were labeled the true values. Deviations from these true values were then studied for the various cases already discussed, and the data were used to obtain conceptual bias estimates. These estimates were then incorporated into the uncertainty equations to study the influence of the conceptual bias terms on the efficiency uncertainty.

Conceptual bias terms needed to be added for $\bar{P}_{01}$, $\bar{P}_{02}$, T_{01}, and T_{02} for the uncertainty study. Hence, the data reduction equation had to be modified to include the conceptual bias terms without altering the original efficiency results. The average value of each property needed for the efficiency calculations can be written as follows (assumed to be the true value with $N = 720$)

$$X_{\text{av}} = \sum_{i=1}^{N} X_i \Big/ N \qquad (9)$$

where X represents $\bar{P}_{01}$, $\bar{P}_{02}$, T_{01}, and T_{02}. Reducing the number of measurements would change the equation to

$$X_{\text{av}} = \sum_{i=1}^{N} X_i \Big/ N + X_C \qquad (10)$$

where N equals the number of measurements and X_C is a dummy value used to implement the conceptual bias estimate. The X_C term is set to zero for all of the averaged properties so that the original

efficiency results are not altered. However, the conceptual bias estimates are added using X_C according to Eqs. (4) and (5).

The thermodynamic efficiency equation was modified to become

$$\eta_{\text{th}} = \frac{(\overline{T_{01}} + T_{01C}) - (\overline{T_{02}} + T_{02C})}{(\overline{T_{01}} + T_{01C})\left\{1 - [(\overline{P_{02}} + P_{02C})/(\overline{P_{01}} + P_{01C})]^{(\gamma-1)/\gamma}\right\}} \tag{11}$$

The new thermodynamic efficiency uncertainty equation then had four new systematic terms,

$$U^2_{\eta_{\text{th}}\text{new}} = U^2_{\eta_{\text{th}}} + \left(\frac{\partial \eta}{\partial P_{01C}} B_{P_{01C}}\right)^2 + \left(\frac{\partial \eta}{\partial P_{02C}} B_{P_{02C}}\right)^2 + \left(\frac{\partial \eta}{\partial T_{01C}} B_{T_{01C}}\right)^2 + \left(\frac{\partial \eta}{\partial T_{02C}} B_{T_{02C}}\right)^2 \tag{12}$$

Table 1 Detailed analysis uncertainty estimates: X

Variable, X	P_X	B_X	U_X
P_{01}, psia, kPa	0.15 (1.0)	0.11 (0.76)	
T_{01}, °R, K	0.71 (0.39)	0.18 (0.10)	
P_{02}, psia, kPa	0.15 (1.0)	0.11 (0.76)	
T_{02}, °R, K			0.74 (0.41)
P_2, psia, kPa			
Cobra			0.30 (2.1)
Regression			0.36 (2.5)
YC			0.54 (3.7)
α_2, deg			
Cobra			0.50
YC			0.90
Regression			1.0

Table 2 Detailed analysis uncertainty estimates: X_iX_j

Variables, X_iX_j	$B_{X_iX_j}$
$P_{01}P_{01}$, psia, kPa	0.013 (0.090)
$T_{01}T_{01}$, °R, K	0.023 (0.013)
$P_{02}P_{02}$, psia, kPa	0.013 (0.090)
$T_{02}T_{02}$, °R, K	0.023 (0.013)
P_2P_2, psia, kPa	0.013 (0.090)
$\alpha_2\alpha_2$, deg	
Cobra with same cobra	0.25
YC with YC	0.81
$P_{01}P_{02}$, psia, kPa	0.013 (0.090)
$P_{01}P_2$, psia, kPa	0.013 (0.090)
$P_{01}\alpha_2$, psia, kPa	0.00 (0.00)
$P_{02}P_2$, psia, kPa	0.013 (0.090)
$P_{02}\alpha_2$, psia, kPa	0.00 (0.00)
$T_{01}T_{02}$, °R, K	0.023 (0.013)
$P_2\alpha_2$, psia, kPa	0.00 (0.00)

The uncertainty estimates are listed in Tables 1 and 2. Standard uncertainty methods were used to obtain these estimates.[5,15,16] The uncertainty estimates for the static pressure and flow angle at the turbine exit varied depending on the region: cobra probe measurements, YC probe measurement, or linear regression region (Fig. 4).

The conceptual bias estimates for the measurement reduction cases were taken from the efficiency comparison results. The differences between the measurement reduction averages and the true averages were taken as the values for conceptual bias estimates. The inlet total pressure and total temperature measurements showed very little spatial variation, and the averaged values for different data reduction cases were equal. Therefore, the conceptual bias estimates were insignificant at the turbine inlet because of the relatively uniform flowfield. The exit total temperature and exit total pressure were the only properties that had significant conceptual bias errors. The conceptual bias estimates for all cases are given in Table 3.

The wall static pressure averaging techniques also required conceptual bias estimates for the turbine exit static pressure. The conceptual bias was considered an additional elemental uncertainty source for the static pressure.[9,15] The conceptual bias estimates for wall static pressure averaging and the overall uncertainty estimates for the static pressure measurements are included in Tables 4 and 5. The conceptual bias terms were large and dominated all other terms for all cases.

Table 4 Static pressure measurement systematic uncertainty estimates

Uncertainty	Elemental error estimates, psia, kPa
Quartz X-ducers	0.025 (0.17)
Barometer, (Calibration)	0.098 (0.68)
Barometer (readings)	0.050 (0.34)
Conceptual bias	
Square volute	3.22 (22.2)
Circular volute	2.95 (20.3)

Table 3 Uncertainty results summary with conceptual bias estimates

	$U\eta/\eta$ %		P_{02}, psia, kPa		T_{02}, °R, K	
Points	Square	Circular	Square	Circular	Square	Circular
Mass average: 360 deg. coverage						
720	0.17	0.17	0.00 (0.00)	0.00 (0.00)	0.00 (0.00)	0.00 (0.00)
360	0.65	0.66	0.01 (0.07)	0.00 (0.00)	0.04 (0.02)	0.02 (0.01)
180	1.40	1.43	0.02 (0.14)	0.00 (0.00)	0.03 (0.02)	0.02 (0.01)
90	2.89	2.94	0.10 (0.69)	0.06 (0.41)	0.13 (0.07)	0.03 (0.02)
Two quadrants (YC)						
720	0.41	0.18	0.08 (0.55)	0.02 (0.14)	0.14 (0.08)	0.03 (0.02)
360	0.76	0.69	0.09 (0.62)	0.02 (0.14)	0.15 (0.08)	0.05 (0.03)
180	1.46	1.45	0.07 (0.48)	0.03 (0.21)	0.14 (0.08)	0.05 (0.03)
90	2.88	2.94	0.06 (0.41)	0.06 (0.41)	0.09 (0.05)	0.04 (0.02)
Two quadrants (cobra)						
720	2.76	0.30	0.74 (5.1)	0.08 (0.55)	0.69 (0.38)	0.05 (0.03)
360	2.90	0.71	0.76 (5.2)	0.08 (0.55)	0.71 (0.39)	0.06 (0.03)
180	3.08	1.47	0.74 (5.1)	0.08 (0.55)	0.70 (0.39)	0.06 (0.03)
90	3.90	2.94	0.74 (5.1)	0.08 (0.55)	0.53 (0.29)	0.02 (0.01)
Area average: 360 deg coverage						
720, 360, 180, 90	8.00	7.50	2.50 (17.2)	1.88 (13.0)	2.50 (1.39)	1.85 (1.03)
Two quadrants (YC)						
720, 360, 180, 90	8.00	7.50	1.75 (12.1)	1.88 (13.0)	2.50 (1.39)	1.95 (1.08)
Two quadrants (cobra)						
720, 360, 180, 90	8.00	7.50	2.04 (14.1)	1.88 (13.0)	2.50 (1.39)	1.95 (1.08)

Results

Turbine Flowfield Mappings

To more fully understand the results of the data studies, the mappings of the measured quantities at the turbine inlet and exit planes will be discussed first.[9,13,14] The flowfield mappings of the OTTR with the both the square and circular exit volutes using the rakes and three-hole probes included turbine inlet and exit total pressure distributions, inlet and exit total temperature distributions, exit static pressure distribution, and exit yaw angle distribution. The 720-point measurements were plotted vs circumferential location for each variable to show clearly both radial and circumferential variations. Exit mass flow rate distributions were then calculated from the measured values. Figures 5 and 6 show the exit mass flow rate distributions for the square and circular volute tests, respectively. The data in Figs. 5 and 6 use all 720-point measurements.

Table 5 Static pressure measurement random and overall uncertainty estimates

Uncertainty	NWA, psia, kPa	CWA, psia, kPa
Random		
Precision of average for Square volute	0.090 (0.62)	0.21 (1.5)
Precision of average for Circular volute	0.060 (0.41)	0.12 (0.83)
Overall for wall static pressure averaging		
Square volute	3.26 (22.5)	3.26 (22.5)
Circular volute	2.98 (20.5)	2.98 (20.5)

The mappings help to understand the relative spatial variations in the turbine inlet and exit flowfields for the square and circular exit volute tests, the effects of these spatial variations on the average values calculated at the turbine inlet and exit planes, and the effects of these average values on turbine efficiency. The mappings for the measured variables ($\bar{P}_0$, T_0, $\bar{P}$, and α) revealed that the turbine inlet had relatively low spatial variations but that the turbine exit had high radial and circumferential spatial variations in all measurements for both tests.[9,13,14] These spatial variations in the measured variables translated into large differences in flow distribution at the turbine exit (Figs. 5 and 6). The mass flow spatial variations alert one to the dangers of area averaging this data. There were especially large spatial variations in exit static pressure just after the exit volute tongue location of 220 deg. The spatial variations were well defined for all measured variables for both tests with the 720-point measurements. The consequences of reducing the number of measurements on defining these spatial variations and the resulting

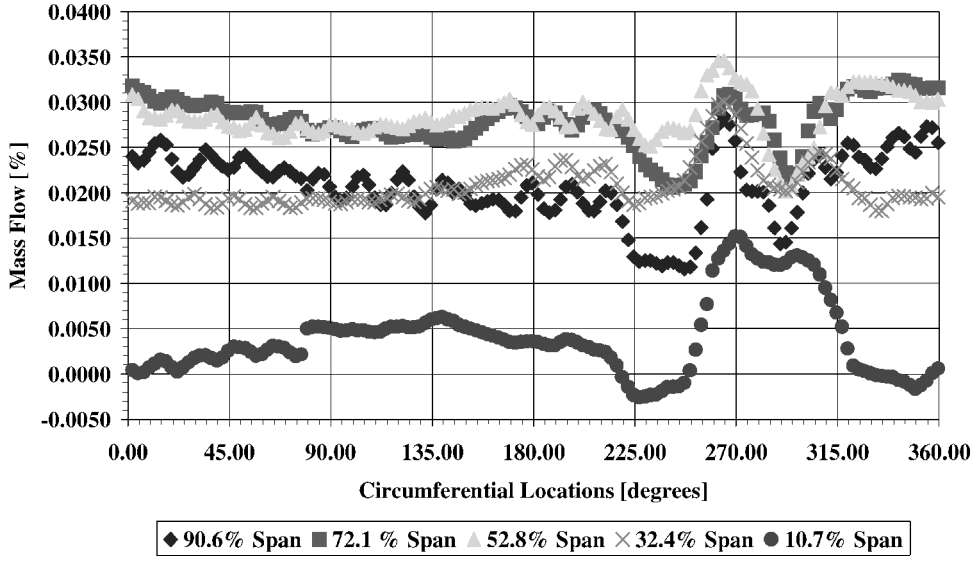

Fig. 5 Turbine exit mass flow distribution (square volute, 720 points).

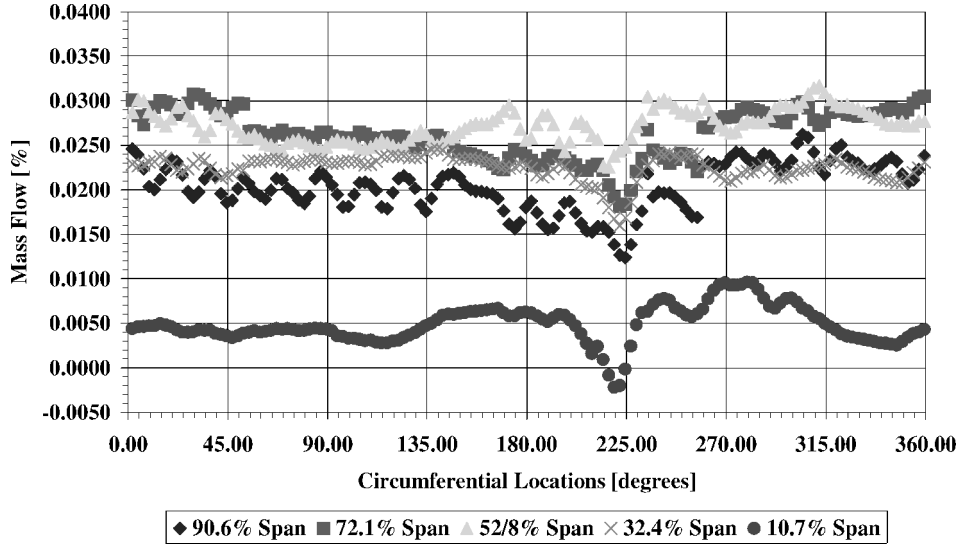

Fig. 6 Turbine exit mass flow distribution (circular volute, 720 points).

effect on turbine efficiency and its uncertainty will be seen in the data reduction studies.

The spatial variation for each flowfield was quantified to provide a feel for the relative differences in the spatial variations and to provide a means of applying the results to future tests. To do this, the spatial variation was defined as follows:

$$\text{spatial variation}(\%) = \frac{\text{max measured value} - \text{min measured value}}{\text{average value}} \times 100 \quad (13)$$

The spatial variations are given in Table 6. As expected, the results show that the spatial variations are very low at the turbine inlet relative to the turbine exit. Also, the spatial variations were larger at the turbine exit with the square volute than they were for the circular volute, as anticipated. (Realize that the same definition must be used to compare various cases for a particular measurement.)

Data Studies

The uncertainty results with error bands generated from mass averaging for the thermodynamic efficiency are summarized in Fig. 7 for the square volute test and in Fig. 8 for the circular volute test. The uncertainty results with error bands generated from area averaging for the thermodynamic efficiency are summarized in Fig. 9 for the square volute test and in Fig. 10 for the circular volute test. The uncertainty results for the two tests were very similar. These results will be used to explain the data studies.

Averaging Techniques

The comparison between mass and area averaging for the two tests generated the same conclusions. The major difference between the two tests was that the circular volute test efficiencies were higher. There were only minor differences in the uncertainty results.

The comparison between mass and area averaging showed that the area averaging, as expected, generated large overall uncertainties U_η (Figs. 9 and 10, Table 3). This was expected due to the large mass flow spatial variations in Figs. 5 and 6. The uncertainty values were large for area averaging even with the maximum number of data points. The mass averaging results gave much lower uncertainty values (Figs. 7 and 8, Table 3). The mass flow near the turbine i.d. was very low, and the measurements were significantly different from those for the rest of the flowfield. Mass averaging correctly accounted for the spatial variations in the exit flowfield by weighting each measurement properly to obtain the average value. The area averaged results had higher uncertainties because the turbine exit flowfield average values had large errors. That is, the area averages did not account for the influence of spatial variations in the turbine exit flowfield; therefore, the area averaged values were very different from the true values. The area averaging ignored the impact of mass flow rate; hence, the area averaging generated higher uncertainties.

Table 6 Flowfield spatial variations

Variables	Spatial variation, % Square	Circular
P_{01}	7.03	7.15
T_{01}	0.65	0.65
P_{02}	37.6	29.6
T_{02}	3.99	3.59
P_2	58.1	35.9
α_2	52.3	37.3

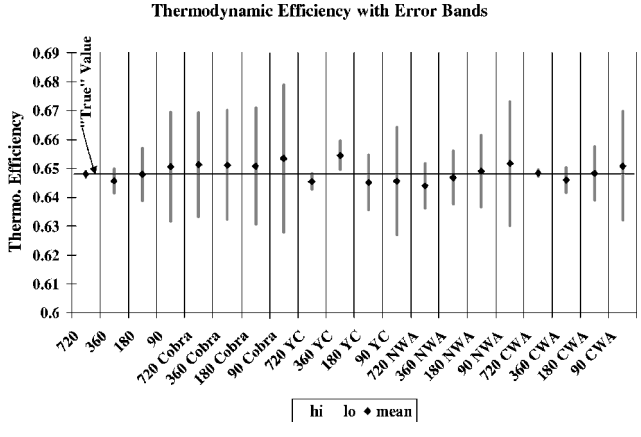

Fig. 7 Uncertainty results for OTTR with square volute (mass averaging).

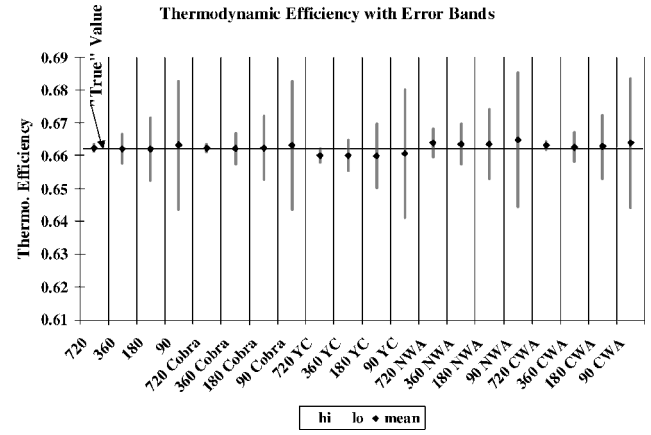

Fig. 8 Uncertainty results for OTTR with circular volute (mass averaging).

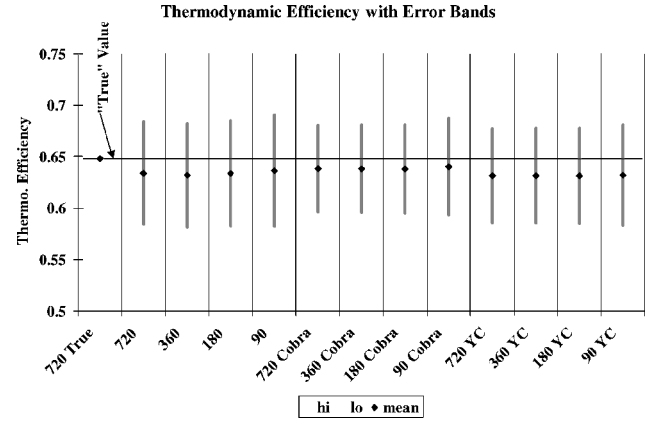

Fig. 9 Uncertainty results for OTTR with square volute (area averaging).

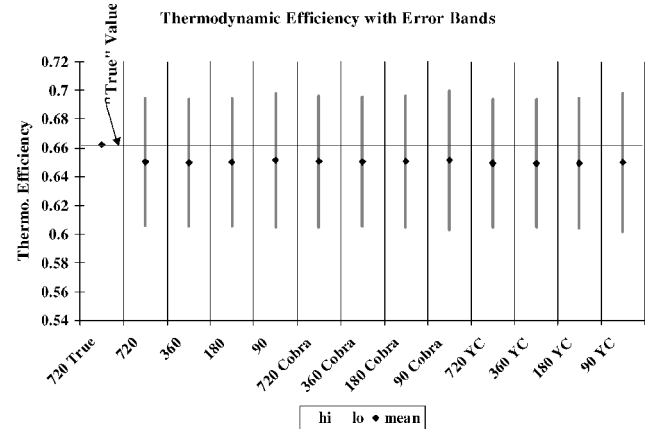

Fig. 10 Uncertainty results for OTTR with circular volute (area averaging).

The averaging techniques analysis proved that mass averaging is crucial for turbine systems that generate high spatial variations in the flowfield. Area averaging was not suitable for the OTTR turbine exit flowfield with its large spatial variations and low uncertainty requirements. Area averaging should only be applied when the flowfield is relatively uniform or when the uncertainty requirements are much less strict.

Reducing Number of Measurements

Results from reducing the number of measurements were compared with the true values obtained using 720-point measurements and mass averaging at the turbine exit. The overall uncertainty percentages for 720-point measurements were approximately ±0.17% of the thermodynamic efficiency for both tests (Table 3). The uncertainty band increased as the number of measurements decreased when mass averaging was used at the turbine exit (Figs. 7 and 8). This increase in uncertainty was due to the uncertainty contribution of the conceptual bias terms. Remember that the conceptual bias was estimated by comparing the average value for the particular case with the true value defined earlier. As the number of measurements decreased, the difference between the average value and the true value increased, causing the conceptual bias estimates to increase (Table 3).

The results proved that the reduction of measurements to 360 points maintained an accuracy below the 1% goal set for the OTTR tests. An important fact was that the entire circumferential area of the turbine exit flowfield was mapped. (This will become clearer when the quadrants coverage cases are discussed.) The full coverage kept the uncertainty low as the number of measurements was reduced to 360 points. Details of the spatial variations from the flowfield maps were maintained with the 360 points; therefore, the average values were still close to the true values, and the conceptual bias estimates were low. The 180-points and 90-points test cases were quite good, but they exceeded the OTTR test accuracy requirement. The uncertainties increased for these cases due to the loss of detail in defining the spatial variations. This resulted in larger differences between the average values and true values and, hence, larger conceptual bias estimates (Table 3).

The averaging of two 90 deg quadrants of the turbine exit plane gave unpredictable results. For the square exit volute test, the uncertainty increased as the number of measurements decreased for both the cobra probes and YC probe cases, as expected. However, Fig. 7 shows that the cobra averaging uncertainty was much higher than the uncertainty generated by YC averaging. For the circular exit volute test, the averaging of two 90-deg quadrants of the turbine exit plane again gave an increase in uncertainty as the number of measurements decreased. Unlike the square volute test, however, Fig. 8 shows that the cobra averaging uncertainty was similar to the uncertainty trend generated by YC averaging. Also, the results with the largest number of cobra probe measurements generated uncertainties that were very close to the best uncertainties, and the uncertainties with the largest number of YC probe measurements were only slightly higher.

These results show that mapping only certain quadrants in flowfields with large circumferential variations can be very dangerous: The results are not predictable. Caution is advised in generalizing the quadrants results. The unpredictable results obtained from the quadrants averaging indicate that the accuracy of the averaged values are highly dependent on the locations of the measurements relative to the large spatial variations and a means of defining where the measurements should be made was not clear. It seems that it would be extremely difficult to know where to make these measurements based on pretest predictions. Therefore, the recommendation is that it would be much better to cover the full 360 deg even with a smaller number of measurements than it would be to cover only certain quadrants with more dense measurements. It is important to cover the full 360 deg to have confidence in the results.

The uncertainty results for area averaging are given in Figs. 9 and 10. As discussed in the preceding section, the area averages did not use a weighting factor to account for the influence of spatial variations in the turbine exit flowfield; therefore, the area averaged values were very different from the true values. The uncertainty results showed that weighting all measurements equally generated a relatively constant uncertainty band, and this band was always much greater than the test goal of 1%. With the area averaging weighting all measurements equally, the average values were approximately the same regardless of the number of measurements taken. The number of measurements did not significantly affect the area averaged values; therefore, the difference between these values and the true value remained approximately constant. Hence, the conceptual bias estimates remained constant (Table 3). These conceptual bias terms were the driving terms in the uncertainty analyses accounting for approximately 90% of the overall uncertainty. The observations confirmed that area averaging offered little account of the effects of large spatial variations in the turbine flowfield.

Evaluation of Measurement Types

The uncertainty results for using wall static pressures to mass average the turbine exit quantities are summarized in Figs. 8 and 9. The wall static pressures were averaged and used to replace the static pressure measurements across the annulus at the turbine exit provided by the cobra and YC probes. The measurement reduction cases for both wall-static averaging methods (NWA and CWA) were done. The uncertainty results showed that the efficiency uncertainty increased and exceeded the OTTR test goal of 1% for NWA; however, the CWA efficiency uncertainties were similar to those of the original uncertainty methodology provided in the first four columns of Figs. 8 and 9. The CWA captured the relative changes in static pressure circumferentially because the o.d. wall static pressure taps were located on the rotating ring. These circumferential changes in static pressure were very similar at all radial positions, although the absolute level of the static pressure varied with radial position. The relative changes in static pressure rather than the absolute level were important in obtaining accurate mass averaged values. The NWA approach did not capture the circumferential variations. Therefore, the CWA mass averaged quantities and efficiency calculations were very close to the true values, resulting in low efficiency uncertainties, whereas the NWA values differed significantly causing the uncertainties to increase. Future static pressure measurements needed for turbine efficiency calculations in flowfields with large spatial variations could be obtained by measuring wall static pressures if enough circumferential measurements can be made. This would save time and money by reducing the number of probe calibrations and the test time required to obtain the necessary measurements.

Eliminating the need to use three-hole probes for static pressure measurements greatly reduces the calibration requirements relative to their use for flow angle measurements only. However, reducing the need for 360-deg coverage with flow angle measurements would provide further benefits. Initial results from a simple sensitivity study for flow angle showed that the efficiency calculation was not extremely sensitive to flow angle. Therefore, obtaining flow angles in limited regions where access with cobra probes on radial actuators is possible, making the flow angle measurements relatively quick and easy to obtain, may be all that is needed. However, further study in required to draw a firm conclusion. Caution is advised when deciding if static pressure and flow angle measurements across the annulus are necessary for a particular test. Remember that this study looked at the effect on turbine efficiency only. Obtaining these measurements would most likely be necessary for complete flowfield maps and code validation.

Turbine Testing Guidelines

Guidelines for future turbine test requirements were compiled based on the analyses of the data studies. For the OTTR, mass averaging of all turbine exit data was needed to maintain accuracy. In addition, only 360-point measurements were needed to maintain the uncertainty below 1% of the efficiency. Last, circumferential averaging of wall static pressure measurements was sufficiently accurate for the OTTR system.

The OTTR results were generalized to provide recommendations for future turbine systems. Although, in the final analysis, results

will be different from test rig to test rig, these recommendations may be used as a starting point for test planning on any test rig.

1) Mass averaging should be considered for all measurements when the expected flowfield spatial variation is larger than that at the inlet of the OTTR (Table 6). Comparisons of the expected spatial variation to those in Table 6 along with comparisons of the expected uncertainties relative to test goals will influence the decision of whether mass averaging is required.

2) Determine the maximum number of independent measurements possible based on the size of the flowfield and probes to be used. This number divided by two [(maximum number of independent measurements)/2] should be sufficient to obtain highly accurate flowfield maps and efficiency calculations provided other precautions (proper probe sizing, calibration, etc.) have been taken to minimize the uncertainty of the test data. Lower numbers of measurements may also be possible depending on the accuracy requirements for the particular test or program. However, it is important to cover the full 360 deg of the flowfield if significant circumferential spatial variations are expected. Quadrant averaging is not recommended for these cases.

3) Wall static pressure measurements may be used rather than static pressure measurements across the annulus provided that these measurements are sufficient to capture the circumferential spatial variations and that the shape of these circumferential spatial variations is not expected to vary significantly in the radial direction.

The turbine/rig basic geometry, the possible probe sizes, and a prediction of the expected average values and spatial variations for the various measured quantities will be needed to use the guidelines. The geometry allows the flow area to be determined. Probe sizes then allow the determination of the maximum possible number of independent measurements. Predictions of average values and expected variations allow comparisons with Table 6 for the spatial variations.

The information for a particular test must then be evaluated relative to the uncertainty goal. A pretest uncertainty analysis should be conducted, and this analysis must include conceptual bias estimates. The conceptual bias estimates used for this work are listed in Table 3 and should be used to help estimate conceptual bias terms for future tests. These OTTR conceptual bias estimates along with the OTTR spatial variations will provide enough information to obtain reasonable conceptual bias estimates for a new flowfield when predictions for the expected spatial variations in the new flowfield are available.

Conclusions

Armed with the information discussed in the preceding section, decisions can be made on the number and types of measurements required to meet the goals of a specific test or program. Using this information will improve the quality of experimental results, while decreasing time and cost for future programs involving flowfields with large spatial variations. Time and money will not be wasted in making unnecessary measurements. Also, time and money will not be wasted on an entire test program that does not meet the goals of the program. Finally, the implication of the test results will be more fully understood due to the uncertainty analysis application.

References

[1]Horlock, J. H., *Axial Flow Turbines*, Krieger, Malabar, FL, 1966, pp. 29–45.

[2]Hudson, S. T., Johnson, P. D., and Wooler, A., "Baseline Design of the Oxidizer Technology Turbine Rig," *Proceedings of the Advanced Earth-to-Orbit Propulsion Technology Conference*, NASA Marshall Space Flight Center, Huntsville, AL, 1994.

[3]Glassman, A. J., *Turbine Design and Application*, NASA SP-290, 1972.

[4]Rodi, F., Varetti, M., and Tomat, R., "Low Pressure Turbine Testing," CP-293, AGARD, Oct. 1980.

[5]Hudson, S. T., "Improved Turbine Efficiency Test Techniques Based on Uncertainty Analysis Application," Ph.D. Dissertation, Dept. of Mechanical and Aerospace Engineering, Univ. of Alabama, Huntsville, AL, April 1998.

[6]Hudson, S. T., and Coleman, H. W., "Analytical and Experimental Assessment of Two Methods of Determining Turbine Efficiency," *Journal of Propulsion and Power*, Vol. 16, No. 5, 2000, pp. 760–767.

[7]Griffin, L. W., and Huber, F. W., "Turbine Technology Team: An Overview of Current and Planned Activities Relevant to the National Launch System," AIAA Paper 92-3220, July 1992.

[8]Huber, F. W., Johnson, P. D., Montesdeoca, X. A., Rowey, R. J., and Griffin, L. W., "Design of Advanced Turbopump Drive Turbines for National Launch Systems Application," AIAA Paper 92-3221, July 1992.

[9]Heng, B. L., "Evaluating Data Averaging Techniques for High Gradient Flow Fields Through Uncertainty Analysis," M.S. Thesis, Dept. of Mechanical Engineering, Mississippi State Univ., Starkville, MS, Aug. 2001.

[10]Bordelon, W. J., Jr., Kauffman, W. J., Jr., and Heaman, J. P., "The Marshall Space Flight Center Turbine Test Equipment; Description and Performance," American Society of Mechanical Engineers, ASME Paper 93-GT-380, May 1993.

[11]Huber, F. W., Johnson, P. D., and Montesdeoca, X. A., "Baseline Design of the Gas Generator Oxidizer Turbine (GGOT) and Performance Predictions for the Associated Oxidizer Technology Turbine Rig (OTTR)," Pratt and Whitney Aircraft, United Technologies Corp., Rept. SZL:38865.doc to Scientific Research Associates, Inc., West Palm Beach, FL, April 1993.

[12]Hudson, S. T., Johnson, P. D., and Branick, R. E., "Performance Testing of a Highly Loaded Single Stage Oxidizer Turbine with Inlet and Exit Volute Manifolds," AIAA Paper 95-2405, July 1995.

[13]Hudson, S. T., and Montesdeoca, X. A., "Aerodynamic Performance Test Results of Single-Stage Oxidizer Turbine with Volute Manifolds," AIAA Paper 97-3099, July 1997.

[14]Hudson, S. T., Xu, R., and Heng, B. L., "Comprehensive Code Validation Dataset for High Turning Turbine/Volute System," AIAA Paper 2002-4163, July 2002.

[15]Coleman, H. W., and Steele, W. G., *Experimentation and Uncertainty Analysis for Engineers*, 2nd ed., Wiley, New York, 1999.

[16]*Assessment of Experimental Uncertainty with Application to Wind Tunnel Testing*, AIAA Standard S-071A, AIAA, Reston, VA, 1999.